Viscosity of Mono- and Polydisperse Mixtures of Photopolymer and Rigid Spheres for Manufacturing of Engineered Composite Materials Using Vat Photopolymerization

John Reynolds, John Unterhalter, Mathieu Francoeur, Michael Bortner, and Bart Raeymaekers**

Vat photopolymerization (VP) additive manufacturing involves selectively curing low-viscosity photopolymers via exposure to ultraviolet light in a layer-wise fashion. Dispersing filler materials in the photopolymer enables tailored end-use properties, but also increases the viscosity and the timescale associated with interparticle network structural recovery postshear. These rheological properties influence self-leveling and recoating of the liquid photopolymer mixture during VP. Herein, viscosity of photopolymer and rigid spherical glass microparticles (filler) is experimentally determined as a function of filler fraction, filler size distribution (mono- and polydisperse), shear rate, and temperature, which are important VP process parameters. Employing existing viscosity models for mono- and polydisperse polymer mixtures demonstrates that particle–particle interactions and the formation of nonspherical clusters of particles strongly affect the viscosity of both monodisperse and polydisperse mixtures with particle volume fractions > 0.05 due to agglomeration/deagglomeration of clusters at elevated shear rates. Consequently, unmodified viscosity models, which assume uniformly dispersed, rigid, spherical particles, are applicable only for mixtures with particle volume fractions < 0.05. It is shown that modifying model parameters such as the fluidity limit and intrinsic viscosity, which explicitly account for nonspherical clusters of particles, improves agreement between viscosity models and experiments, in particular when using a fractal approach.

1. Introduction

Polymer matrix composite materials consist of a polymer matrix with continuous or discontinuous filler material.[1] Continuous filler materials, such as carbon or glass fiber tow,[2] typically span the entire length of the composite material specimen, and align under mechanical tension during fabrication, e.g., to increase the mechanical properties of the composite in the direction of the filler.[3] In contrast, discontinuous filler materials, such as spherical or high aspect ratio particles,[4] either randomly disperse in the matrix,[5] or orient in specific directions, e.g., driven by forces associated with an external field.[6] The properties of the matrix and filler, the interaction between them, and the spatial organization and orientation of the filler in the matrix determine the properties of the composite material.[7] Thus, changing these parameters allows tailoring the properties of the composite material, and manufacturing functional materials and products that possess specific end-use properties for a variety of engineering applications.[8] For instance,

J. Reynolds, M. Bortner
Department of Chemical Engineering
Virginia Tech
Blacksburg, VA 24061, USA
E-mail: mbortner@vt.edu

J. Reynolds, M. Bortner, B. Raeymaekers
Macromolecules Innovation Institute
Virginia Tech
Blacksburg, VA 24061, USA
E-mail: bart.raeymaekers@vt.edu

J. Unterhalter, M. Francoeur
Department of Mechanical Engineering
University of Utah
Salt Lake City, UT 84112, USA

M. Francoeur
Department of Mechanical Engineering
McGill University
Montréal, QC H3A 0C3, Canada

B. Raeymaekers
Department of Mechanical Engineering
Virginia Tech
Blacksburg, VA 24061, USA

The ORCID identification number(s) for the author(s) of this article can be found under https://doi.org/10.1002/adem.202301630.

DOI: 10.1002/adem.202301630

environmental/toxicology researchers have discovered that introducing a large volume fraction of titanium dioxide during fused filament fabrication (FFF) of polylactic acid composite materials enables selective mitigation of toxic algal blooms.[9] Composite materials also find use in ceramics,[10] rubbers,[11] and cementitious pastes[12] among numerous other applications.

Several research groups have used additive manufacturing (AM), including FFF,[13] direct ink writing (DIW),[13] and vat photopolymerization (VP)[14] to manufacture free-form polymer matrix composite materials with tailored properties. Extrusion-based AM methods, such as DIW and FFF, use a mixture of liquid polymer ink or thermoplastic filament with dispersed filler, respectively, that extrudes onto a build plate, where it solidifies.[13] Alternatively, VP methods such as laser stereolithography (laser-SLA) or digital light processing SLA (DLP-SLA) selectively cure a mixture of liquid photopolymer with dispersed filler using a laser or projection light source to build the free-form geometry in a layer-wise fashion.[14] Combining AM with an external field,[15] including shear,[16] electric,[17] magnetic,[18] and ultrasound wave fields[19–21] allows spatially organizing and orienting the filler within the matrix during the AM process.

However, it is well known that the viscosity of a mixture of polymer and filler increases with increasing filler fraction,[22–24] which may cause the FFF or DIW extruder nozzle to clog.[25,26] Several researchers have also emphasized the importance of photopolymer viscosity during VP. Low-viscosity photopolymer is generally desirable because it ensures that the surface of each new layer self-levels or, alternatively, levels by means of wiper-blade recoating.[27] For instance, reports in the literature suggest limiting photopolymer viscosity to less than 3000 mPa·s,[28] although some authors have suggested even more stringent viscosity requirements of less than 1000 mPa·s.[29] Moreover, viscosity is important when combining VP with an external field to organize and orient the filler in the photopolymer matrix, because the external field must be sufficiently strong to drive the filler through the viscous mixture (see, e.g.,[19,30,31]), i.e., the driving force must overcome the drag force on the filler. Hence, viscosity limits the amount of filler that can be dispersed in the filament (FFF), liquid ink (DIW), or photopolymer (VP) for AM of engineered polymer matrix composite materials. Nevertheless, increasing the filler volume fraction in the matrix of engineered composite materials is of crucial importance for manufacturing of, e.g., structural materials[32,33] and ceramic materials,[10,34,35] where a high filler fraction is often required to obtain desirable properties, including strength, stiffness, and fracture toughness.

Dispersing a large filler fraction in the photopolymer can also elicit other rheological phenomena. For instance, filler agglomeration can give rise to a yield stress, i.e., a minimum stress threshold that must be reached for flow to occur.[36] Upon flow, high shear rates may cause filler alignment and deagglomeration, thus reducing the viscosity of the mixture in the form of shear thinning.[37] Less commonly, flow can also increase the viscosity of the mixture due to filler jamming, which could lead the extruder nozzle to clog during DIW or FFF, or affect self-leveling of the mixture of photopolymer and filler during VP.[38] When flow halts, the viscoelastic properties of the mixture of photopolymer and filler return to their baseline. Typically, the viscosity of shear thinning mixtures increases with time due to reagglomeration of the filler (thixotropy), whereas the viscosity of shear thickening mixtures decreases with time once the jammed filler disperses (antithixotropy).[39] These rheological phenomena impact processability of mixtures of photopolymer and filler during the VP process. Thus, it is paramount to understand the rheological effects of dispersing filler in the photopolymer matrix, in the context of VP of engineered polymer matrix composite materials.

Viscosity models help understand these phenomena. They typically describe the reduced viscosity $\eta_r = \eta/\eta_s$ of monodisperse mixtures as a function of the filler volume fraction Φ, where η is the viscosity of the mixture with $\Phi > 0$ and η_s is the viscosity of the mixture with $\Phi = 0$. We distinguish between dilute ($\Phi < \Phi_x$), semidilute ($\Phi_x < \Phi < p_c$), and concentrated ($p_c < \Phi < \Phi^*$) mixtures.[40] Here, $\Phi_x \approx 0.02$ indicates the filler volume fraction beyond which interactions between particles are non-negligible, and p_c is the geometric percolation threshold, which defines the filler volume fraction when the filler first spans the region or volume in which it is dispersed.[23] Φ^* is the fluidity limit, i.e., the filler volume fraction that causes the mixture to act as a solid, with $\Phi^* \approx 0.64$ for monodisperse rigid spheres, derived from the maximum random packing density.[41]

Such viscosity models take the form $\eta_r \approx (1 + [\eta]\Phi)$ for dilute mixtures ($\Phi < 0.02$) after neglecting higher-order terms.[42] The intrinsic viscosity is $[\eta] = \lim_{\Phi \to 0}[(\eta - \eta_s)/\eta_s\Phi]$[22] and $[\eta] = 5/2$ when considering uniform, rigid, spherical particles, and neglecting electrical charges and attractive forces between neighboring particles.[23] However, when particles interact with each other, one must consider hydrodynamic interactions and the reduced viscosity $\eta_r \approx (1 - \Phi)^{-2.5}$.[43] Batchelor and Green documented the importance of considering higher-order-terms for semidilute mixtures with increasing filler volume fraction ($0.01 < \Phi < 0.10$), and showed that $\eta_r \approx 1 + 2.5\Phi + 5.2\Phi^2$,[44] or when additionally accounting for Brownian motion $\eta_r \approx 1 + 2.5\Phi + 6.17\Phi^2$.[45] For concentrated mixtures, Vand showed that $\eta_r \approx 1 + 2.5\Phi + 7.35\Phi^2$ for $\Phi < 0.25$.[46] Subsequently, Roscoe formulated $\eta_r \approx (1 - 1.35\Phi)^{-2.5}$ to account for the importance of particle collisions in concentrated mixtures ($\Phi < 0.4$).[47] Krieger and Dougherty proposed a semi-empirical viscosity model $\eta_r \approx (1 - \Phi/\Phi^*)^{-[\eta]\Phi^*}$ for $\Phi < 0.43$.[48] Additionally, more recent viscosity models, such as those by Mendoza et al., have further improved the understanding of the viscosity of monodisperse mixtures.[49]

The literature documents that the fluidity limit Φ^* for mixtures with rigid spherical particles is between 0.60 and 0.64, which derives from the maximum random particle packing density.[48] However, Φ^* decreases with increasing particle anisotropy and with the agglomeration of individual particles into anisotropic clusters because the maximum random particle packing density decreases with increasing anisotropy.[23] The fluidity limit Φ^* also increases with increasing shear rate $\dot{\gamma}$ as a result of shear-induced particle ordering.[50] For instance, $\Phi^* \approx 0.64$ when $\dot{\gamma} = 0$, yet increases to $\Phi^* \approx 0.71$ when $\dot{\gamma} \to \infty$,[51,52] indicating that the reduced viscosity of a concentrated mixture decreases with increasing shear rate.

Viscosity models that describe the reduced viscosity of polydisperse mixtures as a function of the filler volume fraction(s) Φ_i and the characteristics of the different particle size distributions d_i are not commonly available. Mooney semi-empirically

showed that for bimodal mixtures, the reduced viscosity is given as $\eta_r = \exp(2.5\Phi_1/(1-k\Phi_1-\Phi_2)) \cdot \exp(2.5\Phi_2/(1-k\Phi_2))$, where Φ_1 and Φ_2 are the filler volume fractions of rigid spherical particles with diameters d_1 and d_2, respectively.[53] The self-crowding factor $1.35 \leq k \leq 1.91$ describes first-order interactions between the particles; its limits derive from a face-centered cubic lattice $k = 1/0.74 = 1.35$ and simple cubic packing $k = 6/\pi = 1.91$. Similarly, Chong et al. empirically determined that $\eta_r = [1 + 0.75(\Phi/\Phi^*)/(1-\Phi/\Phi^*)]^2$ for bimodal mixtures of rigid spherical particles, specifically when 25% of the total particle volume fraction Φ consists of small particles.[54] Farris presented a theoretical study of particle interactions to relate the viscosity of polydisperse mixtures to that of a monodisperse mixture, through an apparent particle volume fraction that relates to the particle volume fractions of the different particle sizes that constitute the polydisperse mixture.[55] Other researchers have also attempted to describe the viscosity of polydisperse mixtures with a modified fluidity limit Φ^* based on the composition of the polydisperse mixture.[56–60] However, all these works are related to mono- and polydisperse mixtures of polymer and filler. To our knowledge, no publications exist that specifically model the viscosity of mono- and polydisperse mixtures of photopolymer and filler, and provide experimental validation through rheology analysis, which is fundamental in the context of using VP to manufacture engineered polymer matrix composite materials.

Thus, the objective of this work is to characterize the viscoelastic properties of monodisperse and polydisperse mixtures of photopolymer and rigid spherical glass microparticles (filler) to understand the impact of filler dynamics on the VP process. We use a viscometer to measure the viscosity of the mixtures of photopolymer and filler as a function of filler fraction, filler size distribution (mono- and polydisperse), shear rate, and temperature. We fit several existing viscosity models for mono- and polydisperse mixtures to the viscosity measurements, and we evaluate their applicability to describing viscosity of photopolymer mixtures, in addition to discussing and implementing modifications to the models. Additionally, we use a torsional rheometer to experimentally probe for the presence of a yield stress, shear thinning/thickening, and thixotropic/antithixotropic effects, which validates and explains the applicability of the viscosity models for the mixtures of photopolymer and filler considered here. The results facilitate tailoring VP process parameters based on changes in viscoelastic properties at operating conditions relevant to VP.

2. Experimental Section

2.1. Materials

We use photopolymer resin (3D Resin Solutions (3DRS) V2) with a viscosity of 0.1 Pa.s and density of 1.11 g cm^{-3} under standard temperature and pressure,[61] and spherical soda lime glass microparticles as filler material. **Figure 1** shows optical microscopy images of the soda lime solid glass microparticles with a density of 2.5 g cm^{-3}[62,63] for each of three different particle diameter distributions; $3 \leq d_1 \leq 6$ µm (Figure 1a, Cospheric P2011SL-2.5 3–6 µm), $38 \leq d_2 \leq 45$ µm (Figure 1b, Novum glass T-38-45), and $212 \leq d_3 \leq 250$ µm (Figure 1c, Novum glass T-212-250). Figure 1d–f shows optical microscopy images of different particle volume fractions ($\Phi = 0.01, 0.05, 0.25$) of spherical glass microparticles with diameter d_3, dispersed in the photopolymer. A tip sonicator (Hielscher UP 200 Ht, Teltow, Germany) (time = 600 s, power = 25 W) disperses the spherical glass microparticles in the photopolymer prior to characterization, and the optical microscopy images verify that sonication did not physically alter the glass particles. During the viscosity

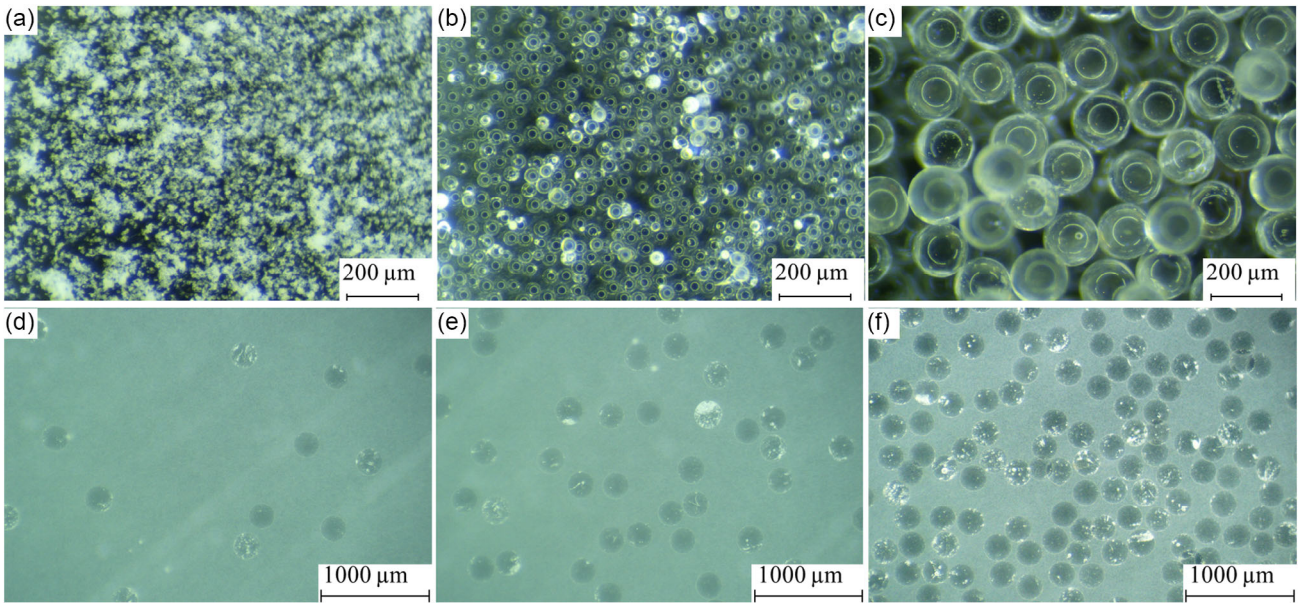

Figure 1. Optical microscopy images of soda lime solid glass microparticles with a) $3 \leq d_1 \leq 6$ µm, b) $38 \leq d_2 \leq 45$ µm, and c) $212 \leq d_3 \leq 250$ µm, and microparticles of diameter d_3 dispersed in photopolymer with d) $\Phi = 0.01$, e) $\Phi = 0.05$, and f) $\Phi = 0.25$ after tip sonication. Images verify that sonication did not alter the glass particles.

experiments, we did not observe substantial precipitation or settlement of particles in the photopolymer.

We determine the effect of particle diameter distribution d_1, d_2, and d_3 on the viscosity and rheological properties of monodisperse mixtures of photopolymer and glass microparticles for particle volume fractions $\Phi = 0.01$, 0.05, and 0.25. We also evaluate the effect of temperature on viscosity. Similarly, we determine the effect of particle size ratio u, defined as the ratio of the large and small mean particle diameter ($u = 231/41.5 = 5.57$, $41.5/4.5 = 9.22$, $231/4.5 = 51.33$) on the viscosity and rheological properties of polydisperse mixtures of photopolymer and glass microparticles. We perform all viscosity and rheology measurements of polydisperse mixtures at room temperature and maintain a constant total particle volume fraction $\Phi = 0.25$. However, we modify the fraction of small microparticle size $\Phi_s = 5\%$, 25%, 50%, 75%, and 95%, within $\Phi = 0.25$. We note that monodisperse mixture comprises photopolymer with glass microparticles of uniform size. However, in practice, $3 \leq d_1 \leq 6$ μm, $38 \leq d_2 \leq 45$ μm, and $212 \leq d_3 \leq 250$ μm are distributed between narrow limits. Hence, in this work, we define monodisperse and polydisperse mixtures as mixtures of photopolymer with one (monodisperse) or two (polydisperse) different size distributions of glass microparticles.

2.2. Plate Rheology Measurement Setup

We use a torsional rheometer (TA Instruments ARES-G2, Newcastle, DE, USA) with 25 mm stainless steel parallel plates and a 1 mm gap to measure yield stress, shear thinning/thickening, and hysteresis of mono- and polydisperse mixtures of photopolymer and microparticles. First, we perform oscillatory strain measurements $0.01 \leq \gamma \leq 100\%$ at $1\ s^{-1}$ to determine the linear viscoelastic region (LVR), and identify the presence of a yield stress. Second, we evaluate the presence of shear thinning using small oscillation measurements with frequency $0.1 \leq \omega \leq 100$ RAD s^{-1} at a strain $\gamma = 0.1\%$, which is within the LVR, such that any deformation of the mixture of photopolymer and microparticles is entirely reversible. Third, we conduct three-interval thixotropy measurements under steady shear rotation conditions, by imposing stepwise changes of the shear rate $\dot{\gamma}$. Initially, we impose $\dot{\gamma} = 1\ s^{-1}$, followed by $\dot{\gamma} = 50\ s^{-1}$, and finally return to $\dot{\gamma} = 1\ s^{-1}$, with each interval covering 30 s. The three-interval method is relevant to the wiper-blade recoating process during VP, which levels a new liquid photopolymer layer upon the previously solidified layer, and has also been previously utilized for glass-filled photopolymers in the context of VP.[64–66]

2.3. Couette Fixture Measurement Setup

We use a disc-style spindle viscometer (Anton Paar, ViscoQC 300, Graz, Austria) to measure the viscosity of monodisperse mixtures of photopolymer and microparticles, for a steady shear rate of $0.016\ s^{-1} \leq \dot{\gamma} \leq 2.500\ s^{-1}$. A heat source and thermometer (Anton Paar, Pt-100, Graz, Austria) control the temperature of the measurement (room temperature ≈25, 40, 60, 80 °C). These parameter ranges capture VP processing conditions.[15] We perform three repetition measurements and report the mean, maximum, and minimum. To measure the viscosity of the polydisperse mixtures of photopolymer and microparticles, we use a steady shear rate $0.016\ s^{-1} \leq \dot{\gamma} \leq 1.500\ s^{-1}$. We determine that six repetitions experiments are required to obtain statistically significant results, based on the standard deviation of a series of trial viscosity measurements, and we report the mean, maximum, and minimum. Note that we use a viscometer with a different geometry than the rheometer of Section 2.2 because a viscometer is typically two orders of magnitude less expensive than a rheometer and, thus, more accessible to researchers, industry, and VP practitioners. Like a rheometer, a viscometer measures viscosity, but with a reduced range of shear rates compared to a rheometer, and without the ability to determine viscoelastic properties such as the storage G' and loss G'' modulus of the mixture of photopolymer and microparticles. However, the reduced range of strain rates in the viscometer measurements still covers shear rates relevant to wiper-blade recoating during VP.

We apply the Weissenberg–Rabinowitsch–Mooney correction to all viscosity measurements to account for the non-Newtonian nature of the mixture of photopolymer and microparticles.[67] We also determine the reduced viscosity, which is the ratio of the viscosity of the mixture of photopolymer and microparticles and the viscosity of the neat photopolymer.

A multiway ANOVA and Tukey's honestly significant difference test determines the statistical significance of the effects of particle volume fraction, temperature, and particle size distribution on the viscosity of the mixture of photopolymer and glass particles. We verify that the log-transformed dataset satisfies the assumptions that residuals are independent, homoscedastic, and follow a normal distribution. We use a p-value of less than 0.05 to indicate statistical significance.

3. Results and Discussion

3.1. Monodisperse Mixtures

3.1.1. Plate Rheology Measurements

Figure 2 shows the storage modulus G' as a function of strain γ for all combinations of particle diameter (marker color: black d_1,

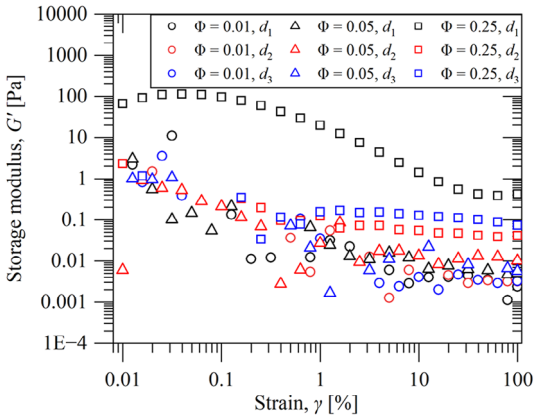

Figure 2. Storage modules G' as a function of strain γ for monodisperse mixtures of photopolymer with different combinations of particle diameter d_i (marker color) and particle volume fractions Φ (marker type).

red d_2, and blue d_3) and particle volume fraction (marker style: circle $\Phi = 0.01$, triangle $\Phi = 0.05$, and square $\Phi = 0.25$) to evaluate yield stress development, and to quantify the maximum strain that renders any deformation reversible. From Figure 2, we observe that mixtures with $\Phi = 0.01$ and 0.05 do not exhibit any substantial yield stress, and the LVR extends past strain $\gamma = 100\%$, independent of the particle diameter d_i. Moreover, the storage modulus G' appears independent of particle diameter regardless of strain, which indicates that weak interparticle networks form at $\Phi \leq 0.05$ within the strain range we evaluate. However, we also observe from Figure 2 that mixtures with $\Phi = 0.25$ show substantially larger storage modulus G' values than those for $\Phi \leq 0.05$. Weak electrostatic (Van der Waals) forces cause particles to establish strong interparticle networks, which increases the elasticity of the mixtures.[68] These observations are accentuated for the smallest particle diameter d_1, which is the only mixture (d_1, $\Phi = 0.25$) in our experiments to exhibit a yield stress (local maximum in G' as a function of γ). In this experiment, the LVR extends to strains of approximately $\gamma = 0.1\%$, which suggests that measurements beyond $\gamma > 0.1\%$ cause deagglomeration of the particles, and temporary destruction of the interparticle network.[68]

Figure 3 shows the complex viscosity η^* as a function of the angular frequency ω for all combinations of particle diameter (marker color: black d_1, red d_2, and blue d_3) and particle volume fraction (marker style: circle $\Phi = 0.01$, triangle $\Phi = 0.05$, and square $\Phi = 0.25$), and for strain $\gamma = 0.1\%$ to remain within the LVR, such that any deformation is reversible, and insignificant deagglomeration of particles occurs. From Figure 3, we observe that the complex viscosity is almost independent of the frequency ω when $\Phi \leq 0.05$, and independent of the particle diameter d_i. These findings highlight the Newtonian flow patterns associated with low particle volume fraction Φ, which do not meaningfully contribute toward viscoelastic behavior. However, the mixtures with $\Phi = 0.25$ and d_2, d_3 show slightly higher complex viscosity than those with $\Phi \leq 0.05$, and the mixture with $\Phi = 0.25$ and d_1 shows the highest complex viscosity, especially at low frequencies. The surface-to-volume ratio increases with decreasing particle diameter and, thus, surface forces enable the development

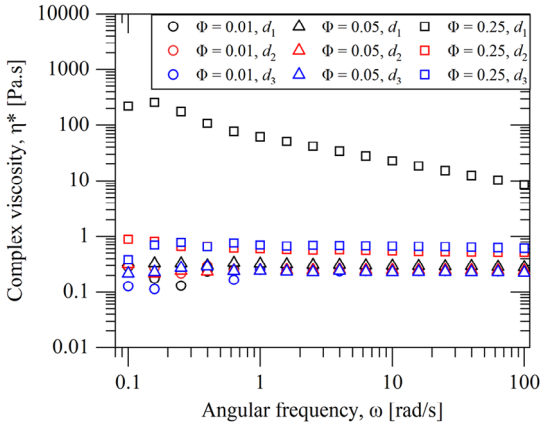

Figure 3. Complex viscosity η^* as a function of frequency ω for monodisperse mixtures of photopolymer with different combinations of particle diameter d_i (marker color) and particle volume fractions Φ (marker type).

of interparticle networks that increase the resistance to flow and, in turn, increase viscosity. We note that the complex viscosity of the mixture with $\Phi = 0.25$ and d_1 also decreases with increasing frequency, which indicates shear thinning, likely due to particle alignment that increases the fluidity of the mixture.[69]

Wiper-blade recoating during the VP process induces deformations larger than those imposed during the torsional rheometer experiments. Although oscillatory measurements provide useful information regarding the presence of interparticle networks, it is also necessary to understand the deformation/reformation of these interparticle networks within the photopolymer mixtures at shear rates that are relevant to the VP process, and also at strains exceeding the LVR defined in Figure 2. The oscillatory measurements shown in Figure 2 and 3 apply small strains, such that any interparticle network deformation is typically small and instantly reversible, depending on shear rate and relaxation. Photopolymer during the VP process, by contrast, does initially not experience strain while at rest in the photopolymer vat. However, it experiences high strains during wiper-blade recoating of a new liquid photopolymer layer on the previously solidified layer. These large strains and shear rates cause rapid deagglomeration of the interparticle network. To mimic this low-high-low strain process, the three-interval thixotropy test imposes stepwise changes of the shear rate at 30 s intervals under steady shear rotation (see Experimental Section), to identify changes of the viscoelastic properties of the mixture of photopolymer and microparticles before and after periods of high strain. Hence, this measurement mimics the wiper-blade recoating during VP at representative shear rates.[65]

Figure 4 shows the viscosity η as a function of time t, for different particle volume fractions (marker style: circle $\Phi = 0.01$, triangle $\Phi = 0.05$, and square $\Phi = 0.25$), and for particle diameter distributions d_1 (Figure 4a), d_2 (Figure 4b), and d_3 (Figure 4c), respectively. We also delineate the time intervals and identify their corresponding shear rate.

From Figure 4, we observe that, as expected, the viscosity η increases with increasing particle volume fraction Φ, independent of the particle diameter d_i. Also, when $\Phi \leq 0.05$, the viscosity is independent of the shear rate, thus suggesting the mixtures of photopolymer and microparticles behave like Newtonian fluids, as also observed in Figure 3. However, when $\Phi = 0.25$, the viscosity of the mixture with particle diameter d_1 (Figure 4a) decreases when the shear rate increases from $\dot{\gamma} = 1\,s^{-1}$ to $\dot{\gamma} = 50\,s^{-1}$ due to shear thinning and deagglomeration of the interparticle network. The viscosity restores to its original value within a short time when decreasing the shear rate to $\dot{\gamma} = 1\,s^{-1}$, as the interparticle network reforms. This thixotropic behavior is common for particle suspensions with sufficiently high particle volume fraction to lead to significant interparticle interactions.[39] The mixture with $\Phi = 0.25$ and d_2 (Figure 4b) exhibits shear thickening, where the viscosity increases with increasing shear rate, which is even more pronounced for the mixture with $\Phi = 0.25$ and d_3 (Figure 4c). However, the latter mixture of photopolymer and microparticles also displays "antithixotropic" behavior, i.e., the viscosity slowly decreases after exposure to elevated shear. Shear thickening can occur because large particles migrate to the edge of the rheometer plate during the high shear interval, which causes them to

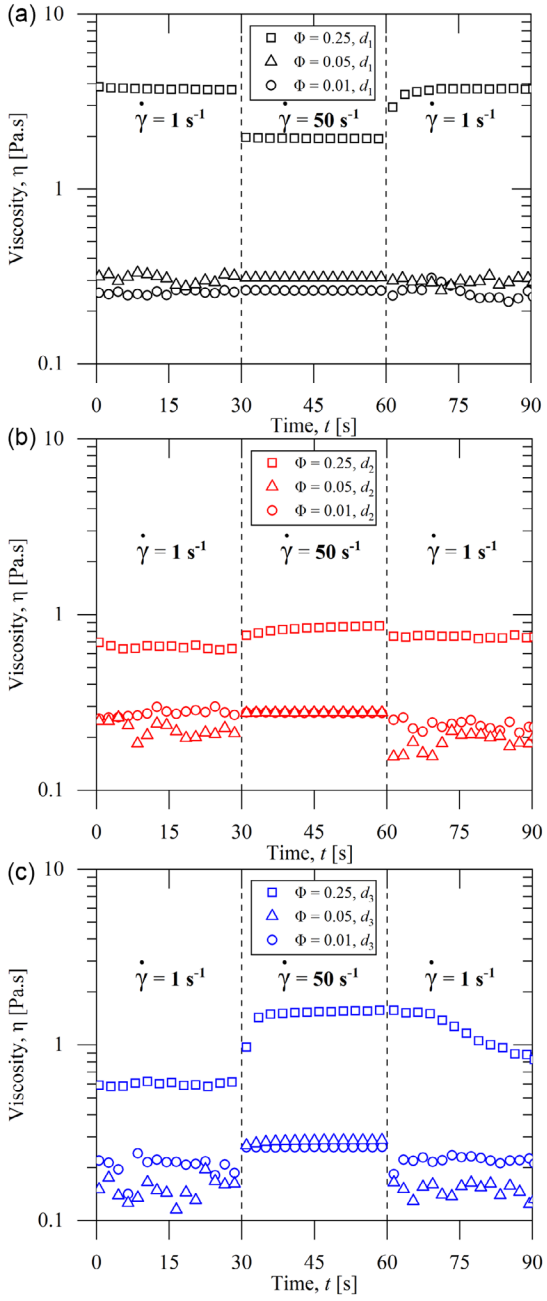

Figure 4. Three-interval thixotropy measurements, showing viscosity η as a function of time t for monodisperse mixtures of photopolymer with different particle volume fraction Φ (marker style) and for different particle, a) $3 \leq d_1 \leq 6$ µm, b) $38 \leq d_2 \leq 45$ µm, and c) $212 \leq d_3 \leq 250$ µm.

agglomerate and increase resistance to flow. Upon reducing the shear rate, particles redisperse in the photopolymer, thus reducing the resistance to flow and viscosity.[70]

3.1.2. Couette Fixture Measurements

Figure 5 shows the reduced viscosity η_r as a function of the shear rate $\dot{\gamma}$ for monodisperse mixtures of photopolymer with particle diameter d_1 and d_3 and for different particle volume fractions Φ.

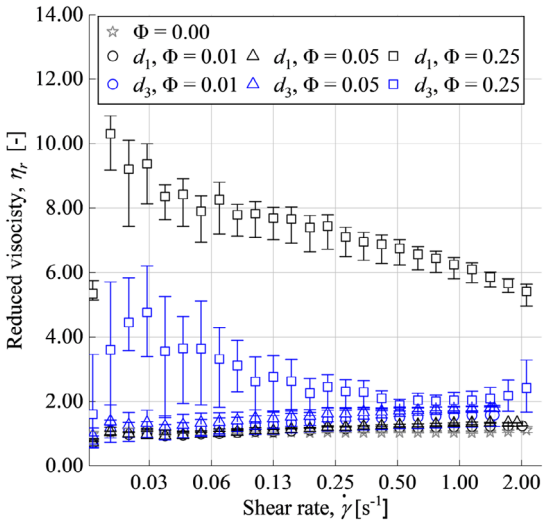

Figure 5. Reduced viscosity η_r of a monodisperse mixture of photopolymer and glass microparticles as a function of the shear rate $\dot{\gamma}$ for different combinations of particle diameter d_i and particle volume fraction Φ. Datapoints represent the average of three measurements, and error bars show the minimum and maximum of each measurement.

These mixtures capture the most extreme effects of the particle diameter on the viscosity of monodisperse mixtures. From Figure 5, we observe that when $\Phi \leq 0.05$, the reduced viscosity η_r increases slightly with increasing shear rate $\dot{\gamma}$ because the neat photopolymer dominates the viscosity of the mixture as few particle–particle interactions occur. Additionally, the reduced viscosity η_r increases with increasing particle size d_i (not statistically significant) and increasing particle volume fraction Φ ($p < 0.05$). Mixtures of photopolymer and microparticles with $\Phi \leq 0.05$ behave as Newtonian fluids, but shear thickening occurs with increasing particle diameter, as illustrated in Figure 4. When considering a large particle volume fraction ($\Phi = 0.25$), the reduced viscosity η_r decreases with increasing shear rate $\dot{\gamma}$, likely because of shear-induced particle ordering, which reduces the effect of particle–particle interactions on the viscosity of the mixture of photopolymer and microparticles.[51,52] However, mixtures with $\Phi = 0.25$ and particle diameter d_3 show that the reduced viscosity η_r increases with increasing shear rate beyond $\dot{\gamma} = 1\ s^{-1}$, which provides evidence that shear thinning occurs when the shear rate $\dot{\gamma} \leq 1\ s^{-1}$, and that particle agglomeration occurs when $\dot{\gamma} > 1\ s^{-1}$. Repeating these measurements at different temperatures yields similar results, but the reduced viscosity η_r decreases with increasing temperature T ($p < 0.05$), in agreement with viscosity measurements of neat photopolymer by Liu et al.[71] We also note that additional viscosity measurements with $0.05 \leq \Phi \leq 0.25$ would reveal the transition between both regimes.

3.1.3. Viscosity Models

We select reduced viscosity measurements for a low ($\dot{\gamma} = 0.028\ s^{-1}$) and high ($\dot{\gamma} = 0.548\ s^{-1}$) shear rate to fit to existing viscosity models for monodisperse mixtures. In the context of

viscometer measurements, the "low" shear rates are representative of Newtonian flow, whereas the "high" shear rates elicit non-Newtonian behavior (see Figure 5). **Figure 6**a shows the reduced viscosity η_r as a function of the particle volume fraction Φ for different combinations of particle diameter d_i and shear rate $\dot{\gamma}$. We superimpose selected viscosity models for a monodisperse mixture of polymer and rigid, spherical particles. We consider the following models (see also Section 1): Einstein[42] and Brinkman,[43] because they are valid for dilute mixtures ($\Phi < 0.01$); Batchelor,[45] because it is suitable for semidilute mixtures as they account for interactions between particles; Krieger and Dougherty,[48] because it considers particles forming doublets (conglomerates of two particles), which we observe in optical microscopy images of our experiments (Figure 1c); and Mendoza et al.[49] and Roscoe,[47] because they consider hard spheres and collisions between particles.

Figure 6a shows good agreement between experimental results and the monodisperse viscosity models with $[\eta] = 2.5$

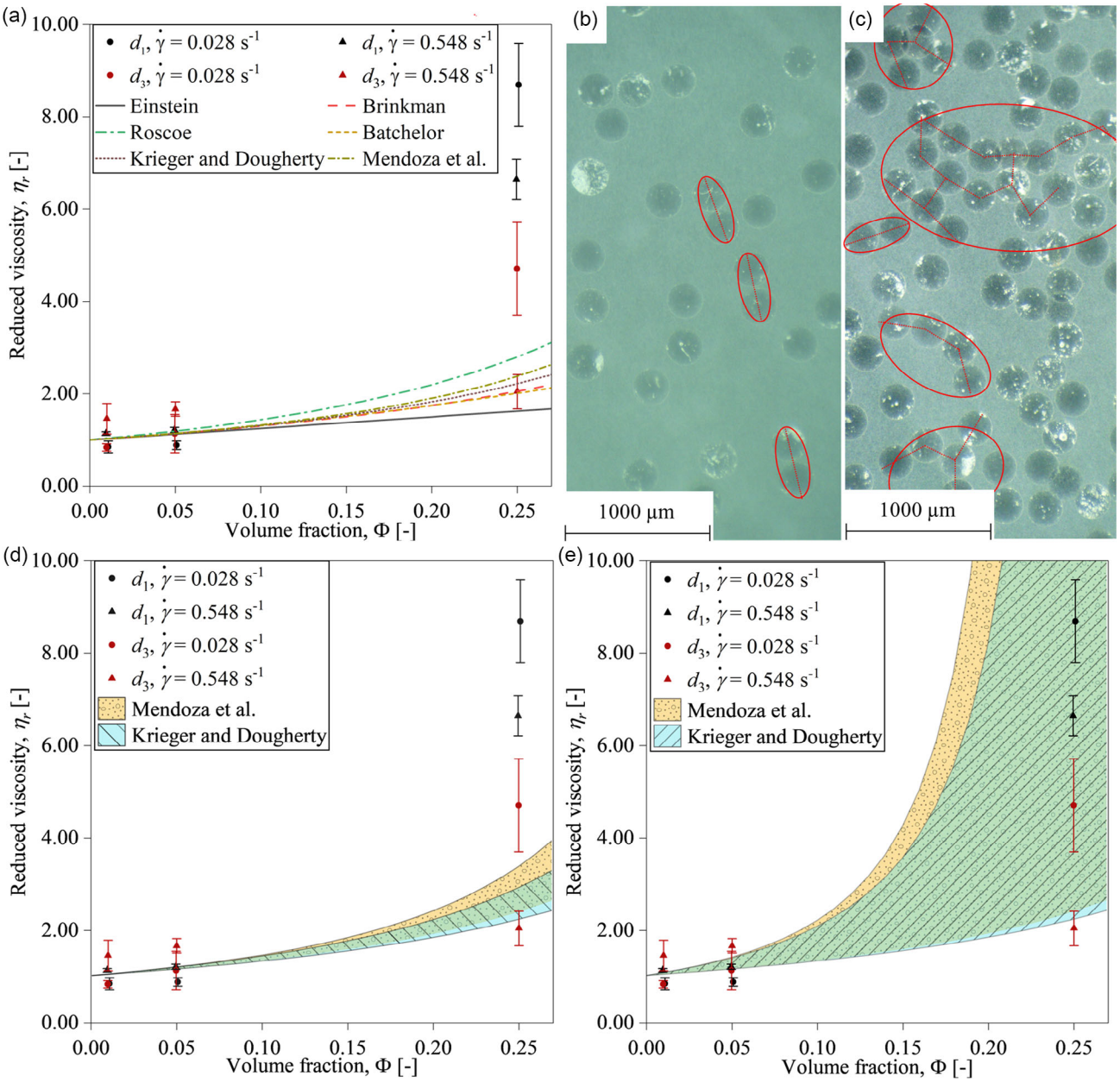

Figure 6. a) Reduced viscosity η_r as a function of the particle volume fraction Φ for different combinations of particle diameter d_i and shear rate $\dot{\gamma}$, with superposition of selected monodisperse viscosity models. Optical microscopy images highlight the nonspherical clusters of spherical particles with red ellipses for b) d_3 and $\Phi = 0.05$ and c) d_3 and $\Phi = 0.25$. Reduced viscosity η_r as a function of the particle volume fraction Φ for different combinations of particle size distribution d_i and shear rate $\dot{\gamma}$, accounting for nonspherical clusters of spherical particles by d) modifying model parameters, and e) using a fractal method, showing the Mendoza et al. (blue envelope) and Krieger and Dougherty models (yellow envelope) superimposed on the experimental results.

and $\Phi^* = 0.64$,[23] for particle volume fractions $\Phi \leq 0.05$ only. However, particles agglomerate in nonspherical clusters. We illustrate examples of nonspherical clusters of spherical particles, marked with red ellipses superimposed on the optical microscopy images (additionally, dashed lines indicate contacting particles within each cluster) in Figure 6b for d_3 with $\Phi = 0.05$, and in Figure 6c for d_3 with $\Phi = 0.25$. The average particle cluster aspect ratio, calculated as the ratio of major and minor axes of the ellipse, is 2.4 ($\Phi = 0.05$) and 1.7 ($\Phi = 0.25$), respectively. Particles are part of a cluster if they contact at least one other particle to form a new nonspherical cluster, or add to the size of an existing nonspherical cluster of spherical particles.

Figure 6d shows the same experimental data as Figure 6a, but we superimpose the Krieger and Dougherty[48] (blue envelope) and Mendoza[49] (yellow envelope) viscosity models for monodisperse mixtures of polymer and rigid, spherical particles, covering $2.50 \leq [\eta] \leq 3.18$ and $0.54 \leq \Phi^* \leq 0.64$ to account for nonspherical clusters of spherical particles dispersed in the photopolymer.[23] The fluidity limit Φ^* decreases with increasing particle (or particle cluster) aspect ratio because the maximum random packing density Φ_m decreases with increasing anisotropy. Hence, we approximate the lower limit of $\Phi^* \approx \Phi_m = 0.54$ for simple cubic packing of spheres.[23] Similarly, $[\eta]$ increases from 2.50 for monodispersed, rigid, spheres to 3.18 for oblong ellipsoids with an aspect ratio of 2.4, as determined from our experimental results.[23] From Figure 6d, we observe that accounting for nonspherical clusters of spherical particles in the theoretical viscosity models for monodisperse mixtures improves their agreement with the experimental results.

Alternatively, one may use a fractal approach to account for nonspherical clusters of spherical particles in the theoretical viscosity models.[72] Figure 6e shows the same experimental data as Figure 6a, but we superimpose the Krieger and Dougherty[48] (blue envelope) and Mendoza[49] (yellow envelope) viscosity models for monodisperse mixtures with rigid, spherical particles, covering $1.00 \leq a_a/a \leq 2.50$, where a and a_a are the radius of a particle and a cluster of particles, and $2.08 \leq D \leq 3$, where D is the fractal index,[72] which represents the dimensions of a Euclidean space.[73,74] The lower bound of D corresponds with results from Aubert and Cannell.[75] Additionally, we approximate the average value of a_a for the nonspherical clusters by determining the radius of the circle with an area equivalent to that of the ellipse that fits the nonspherical cluster of spherical particles. From Figure 6e, we observe that after accounting for nonspherical clusters of spherical particles using the fractal approach, the experimental data falls within the envelope established by the viscosity models based on the respective parameter ranges of a_a/a and D.

3.2. Polydisperse Mixtures

3.2.1. Plate Rheology Measurements

We perform an identical set of rheology measurements for polydisperse mixtures of photopolymer and glass microparticles as we performed for monodisperse mixtures (see Experimental Section).

Figure 7 shows the storage modulus G' as a function of strain γ for different values of the particle size ratio, showing (a) $u = d_2/d_1 = 41.5/4.5 = 9.22$, (b) $u = d_3/d_1 = 231/4.5 = 51.33$, and (c) $u = d_3/d_2 = 231/41.5 = 5.57$, and for constant total particle volume fraction $\Phi = 0.25$. However, we modify the fraction of small particle size $\Phi_s = 5\%$, 25%, 50%, 75%, and 95%, within the total particle volume fraction $\Phi = 0.25$ (marker types and colors). From Figure 7, we observe that $u = 9.22$ (Figure 7a) and

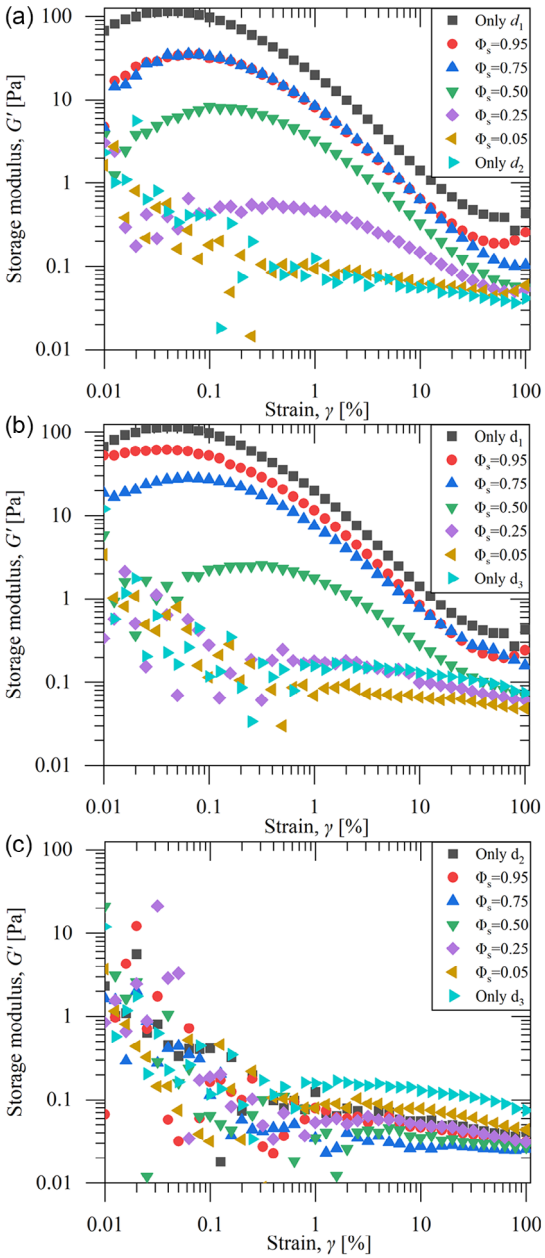

Figure 7. Storage modules G' as a function of strain γ for polydisperse mixtures of photopolymer with different particle size ratios, showing a) $u = d_2/d_1 = 41.5/4.5 = 9.22$, b) $u = d_3/d_1 = 231/4.5 = 51.33$, and c) $u = d_3/d_2 = 231/41.5 = 5.57$, and for constant total particle volume fraction $\Phi = 0.25$. We modify the fraction of small particle size $\Phi_s = 5\%$, 25%, 50%, 75%, and 95%, within $\Phi = 0.25$ (marker types and colors).

$u = 51.33$ (Figure 7b) provide similar results; increasing the particle volume fraction of the smallest particle diameter within a constant total particle volume fraction $\Phi = 0.25$ increases the storage modulus G', independent of strain.

Increasing the volume fraction of small particles Φ_s also decreases the LVR, which suggests that the strain required to disrupt the interparticle network decreases with increasing Φ_s, consistent with earlier results by Willenbacher and Georgieva, as well as Rueda et al.[68,69] In contrast, the LVR and yield stress disappear with increasing particle size, due to decreasing electrostatic forces associated with decreasing surface-to-volume ratio of the particles. This is particularly noticeable when comparing $\Phi_s = 0.25$ in Figure 7a,b; the yield stress is still visible in Figure 7a, but vanishes for $\Phi_s \leq 0.25$ in Figure 7b. This finding is further substantiated in Figure 7c, such that all mixtures of photopolymer and microparticles present similar values of the storage modulus G', independent of Φ_s, which again relates to the decreasing tendency to form an interparticle network with increasing particle diameter.

Figure 8 shows the complex viscosity η^* as a function of angular frequency ω for different values of the particle size ratio, showing (a) $u = d_2/d_1 = 41.5/4.5 = 9.22$, (b) $u = d_3/d_1 = 231/4.5 = 51.33$, and (c) $u = d_3/d_2 = 231/41.5 = 5.57$, and for constant total particle volume fraction $\Phi = 0.25$. However, we modify the fraction of small particle size $\Phi_s = 5\%$, 25%, 50%, 75%, and 95%, within $\Phi = 0.25$ (marker types and colors). The observations of Figure 8 agree with those of Figure 7. Increasing the fraction of small particle size Φ_s within the constant total particle volume fraction $\Phi = 0.25$ increases the viscosity of the mixture and its degree of shear thinning, independent of the frequency. When comparing Figure 8a,b, we observe that $\Phi_s = 0.25$ marks the transition from Newtonian behavior ($\Phi_s \leq 0.25$) to shear thinning ($\Phi_s > 0.25$). Similar to the results of Figure 7c, and 8c shows that all mixtures with $u = 5.57$ behave Newtonian due to a lack of interparticle network formation.

Figure 9 shows the viscosity η as a function of time t, for different values of the particle size ratio, showing (a) $u = d_2/d_1 = 41.5/4.5 = 9.22$, (b) $u = d_3/d_1 = 231/4.5 = 51.33$, and (c) $u = d_3/d_2 = 231/41.5 = 5.57$, and for constant total particle volume fraction $\Phi = 0.25$. However, we modify the fraction of small particle size $\Phi_s = 5\%$, 25%, 50%, 75%, and 95%, within $\Phi = 0.25$ (marker types and colors). We also delineate the time intervals and identify their corresponding shear rate.

From Figure 9, we observe that for all mixtures of photopolymer and microparticles, the viscosity η increases with increasing fraction of small particles size Φ_s during the first interval when $\dot{\gamma} = 1\,s^{-1}$. The surface-to-volume ratio of particles increases with decreasing size and, thus, attractive electrostatic forces increase because they are a function of the particle surface area. Correspondingly, the magnitude of the electrostatic forces increases with increasing Φ_s, which drives the formation of an interparticle network. During the second interval $\dot{\gamma} = 50\,s^{-1}$, Figure 9a,b shows that for $\Phi_s > 0.50$, the mixtures of photopolymer and microparticles show shear thinning and thixotropic behavior due to particle alignment and deagglomeration, respectively. However, when $\Phi_s = 0.50$, the mixtures display neither shear thinning nor thixotropic behavior, which is likely due to the competing effects of shear-induced ordering

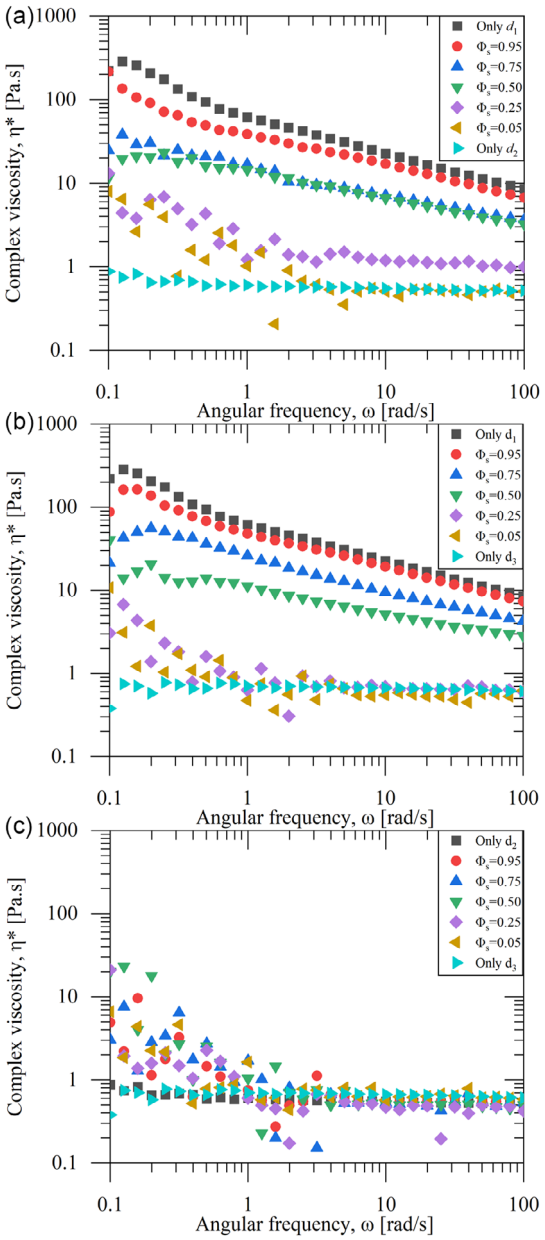

Figure 8. Complex viscosity η^* as a function of angular frequency ω for polydisperse mixtures of photopolymer with different particle size ratio, showing a) $u = d_2/d_1 = 41.5/4.5 = 9.22$, b) $u = d_3/d_1 = 231/4.5 = 51.33$, and c) $u = d_3/d_2 = 231/41.5 = 5.57$, and for constant total particle volume fraction $\Phi = 0.25$. We modify the fraction of small particle size $\Phi_s = 5\%$, 25%, 50%, 75%, and 95%, within $\Phi = 0.25$ (marker types and colors).

of the small and large particle sizes in the polydisperse mixture of photopolymer and microparticles. Clusters of small particles deagglomerate due to high shear, which reduces viscosity (shear thinning), whereas large particles sizes migrate to the edge of the rheometer, which increases viscosity (shear thickening). During the third interval when $\dot{\gamma} = 1\,s^{-1}$, the small particles reagglomerate, which increases viscosity (thixotropy), but the large particles migrate back to the center of the rheometer, which

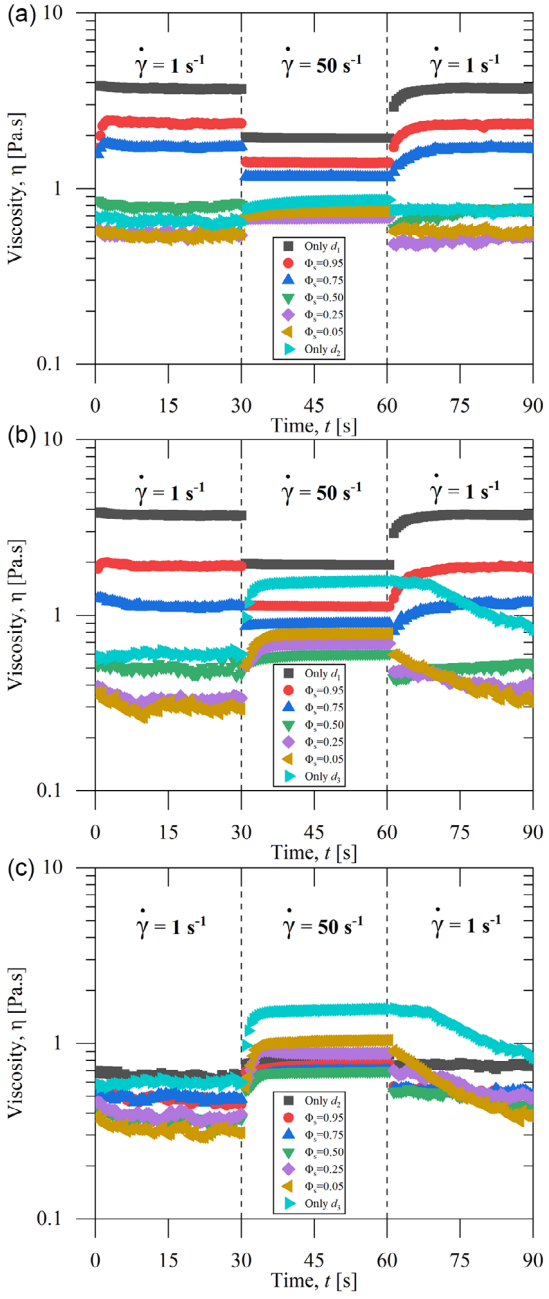

Figure 9. Three-interval thixotropy measurements, showing viscosity η as a function of time t for polydisperse mixtures of photopolymer with different particle size ratio, showing a) $u = d_2/d_1 = 41.5/4.5 = 9.22$, b) $u = d_3/d_1 = 231/4.5 = 51.33$, and c) $u = d_3/d_2 = 231/41.5 = 5.57$, and for constant total volume fraction $\Phi = 0.25$. We modify the fraction of small particle size $\Phi_s = 5\%$, 25%, 50%, 75%, and 95%, within $\Phi = 0.25$ (marker types and colors).

reduces viscosity (antithixotropy). Figure 9c further verifies this finding because the degree of shear thickening/antithixotropy increases with decreasing fraction of small particle size Φ_s.

When considering the rheology results in the context of the VP process, they explain that relaxation of the mixture of photopolymer and microparticles after periods of high shear, in the form of thixotropy/antithixotropy, may negatively impact wiper-blade recoating between subsequent layers. After the wiper-blade shears the liquid mixture photopolymer of photopolymer and microparticles, thixotropic materials remain temporarily fluidic, before settling on the build plate or previously cured layer, whereas antithixotropic materials build structure temporarily before flow initiates. However, Figure 9 illustrates that it is possible to identify the time-scales associated with both relaxation processes, and adjust VP process parameters accordingly. Furthermore, the results highlight that proper selection of particle dispersity is key to formulating mixtures of photopolymer and microparticles for use in VP processes.

3.2.2. Couette Fixture Measurements

We select reduced viscosity measurements for a low ($\dot{\gamma} = 0.028\ s^{-1}$) and high ($\dot{\gamma} = 0.548\ s^{-1}$) shear rate to fit to existing viscosity models for polydisperse mixtures of photopolymer and microparticles, similar to the discussion of the monodisperse mixtures in Section 3.1.2. **Figure 10** shows the reduced viscosity η_r as a function of the volume fraction of small particle size Φ_s for different combinations of particle size ratio u and shear rate $\dot{\gamma}$, for a constant total particle volume fraction $\Phi = 0.25$.

3.2.3. Viscosity Models

We superimpose the Mooney model[53] (purple envelope), which quantifies the reduced viscosity as a function of the composition of concentrated polydisperse mixtures, on the experimental measurements. The self-crowding factor $1.35 \leq k \leq 1.95$ defines the boundaries of the envelope. Markers (b)–(g) refer to the optical microscopy images of each polydisperse mixture of photopolymer and glass microparticles. Note that the optical microscopy images show the mixture at $\dot{\gamma} = 0$ in contrast to the data points in Figure 10a, which are obtained within a flow field.

From Figure 10a, we observe that the reduced viscosity η_r initially decreases with increasing volume fraction of small particle size Φ_s. However, when $\Phi_s > 50\%$, the reduced viscosity η_r increases with increasing volume fraction of small particle size Φ_s, independent of the particle size ratio u and the shear rate $\dot{\gamma}$. A likely cause of this observation is that the fluidity limit Φ^* first increases with increasing Φ_s as the small particles fit within the voids between the large particles, which decreases the reduced viscosity η_r.[54,57,60,76,77] However, further increasing Φ_s leads to agglomeration and jamming of the particles, thus increasing the reduced viscosity η_r; when $\Phi_s > 50\%$, the viscoelastic properties of the polydisperse mixture are increasingly dominated by the fraction of small particles only. Figure 10b–e visualizes particle aggregation with increasing volume fraction of small particle size Φ_s.

Reasonable agreement between the experimental results and the Mooney model only exists when $\Phi_s \approx 50\%$. The Mooney model does not consider nonspherical clusters of particles, which evidently plays an important role in altering viscosity, especially for small particle sizes.

Figure 11 shows the same experimental data as Figure 10a but, instead for $\Phi_s < 25\%$ and $\Phi_s > 75\%$, we superimpose the

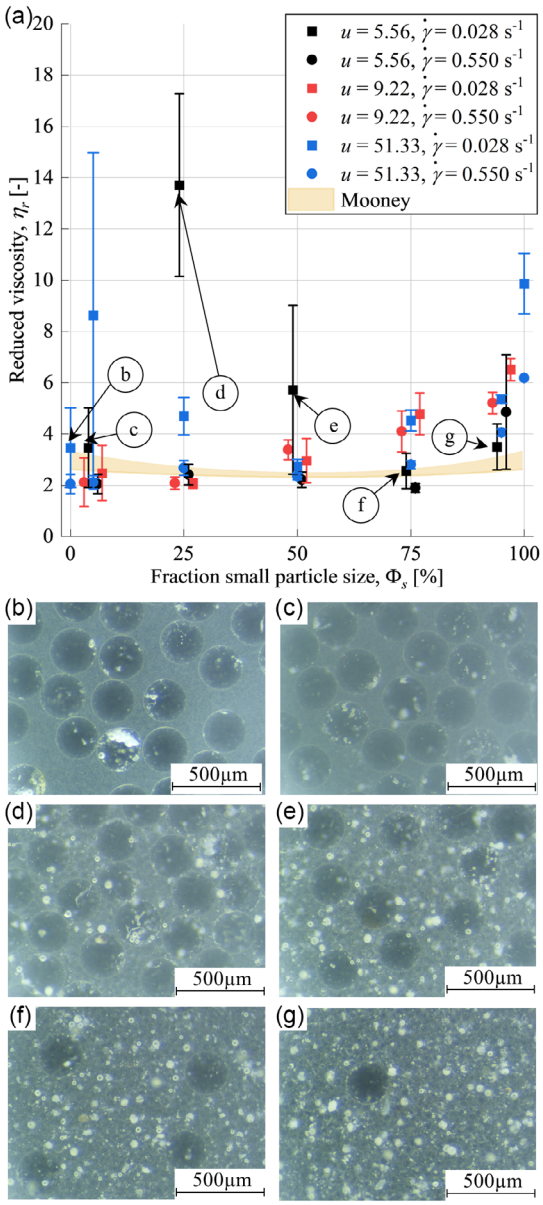

Figure 10. a) Reduced viscosity η_r of polydisperse mixtures of photopolymer and glass microparticles as a function of the fraction of small particle size Φ_s for different combinations of the particle size ratio u and the shear rate $\dot{\gamma}$, and $\Phi = 0.25$. The Mooney model is superimposed (purple envelope) on the experimental data. Optical microscopy images of the polydisperse mixture $u = 5.56$ with b) $\Phi_s = 0\%$, c) $\Phi_s = 5\%$, d) $\Phi_s = 25\%$, e) $\Phi_s = 50\%$, f) $\Phi_s = 75\%$, and g) $\Phi_s = 95\%$ match with data points in (a).

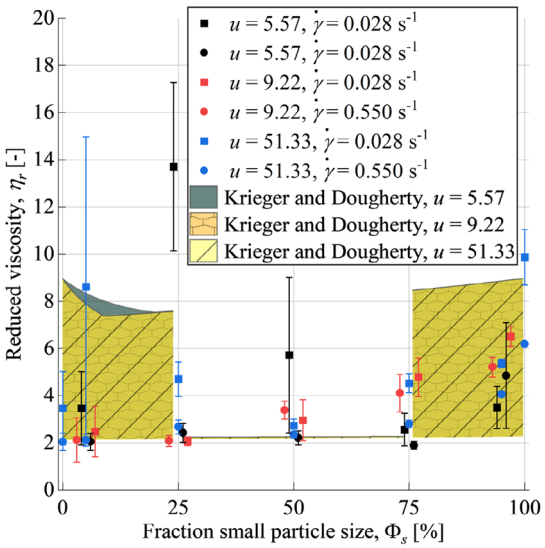

Figure 11. Reduced viscosity η_r as a function of fraction small particle size Φ_s for polydisperse mixtures of photopolymer and glass microparticles for different combinations of the particle size ratio u and the shear rate $\dot{\gamma}$, and $\Phi = 0.25$. We superimpose the Krieger and Dougherty model for $\Phi_s < 25\%$ and $\Phi_s > 75\%$, and for different values of u (green, orange, and yellow envelopes).

Krieger and Dougherty model[48] for particle size ratio $u = 5.75$ (green envelope), $u = 9.22$ (orange envelope), and $u = 51.33$ (yellow envelope), because their viscoelastic properties approach those of a monodisperse mixture. Therefore, it is possible that monodisperse viscosity models such as the Krieger and Dougherty model can still accurately capture the viscosity of the polydisperse mixtures. In these models, we use an effective particle volume fraction $\Phi_a = \Phi/\Phi_m$, where Φ_m is the maximum packing density.[72] In contrast, for $25\% \leq \Phi_s \leq 75\%$, the mixture contains similar amounts of small and large particles and no monodisperse viscosity model should be used. We note that the orange and yellow envelopes almost completely overlap and show as dark yellow in Figure 11.

From Figure 11, we observe that the envelopes that describe η_r based on the Krieger–Dougherty model are almost independent of u. We only observe a small difference for the smallest $u = 5.75$. We note that when the viscoelastic properties of the polydisperse mixture approach those of a monodisperse one, the viscosity is not strongly dependent on the particles size (see Figure 8), which explains why the envelopes almost completely overlap. The upper contour of the envelope slightly decreases with increasing Φ_s when $\Phi_s < 25\%$, and slightly increases with increasing Φ_s when $\Phi_s > 75\%$, similar to the Mooney envelopes in Figure 11. The envelopes contain a majority of experimental data points suggesting that monodisperse models such as the Krieger and Daugherty model can still adequately capture the behavior of polydisperse mixtures. However, the large area of the envelopes makes drawing conclusions difficult in this context, suggesting that future improvements are necessary to capture the complex fluid flow of polydisperse mixtures of photopolymer and filler.

4. Conclusion

The need for high viscosity mono- and polydisperse mixtures of photopolymer and filler for VP of engineered polymer matrix composite materials requires understanding their process–structure–property relationships to enable tailoring VP process parameters. The combination of plate rheology and Couette

fixture measurements with theoretical models closes this knowledge gap by providing a fundamental understanding of the interplay between resistance to flow, subsequent timescales for recovery, and its effect on wiper-blade recoating during the VP process. We considered mixtures of photopolymer and spherical glass microparticles and modified their total particle volume fraction, particle size distribution (mono- and polydisperse), temperature, and shear rate. The results are generalizable to a broad spectrum of photopolymer mixtures for VP. We conclude that: 1) Particle–particle interactions, the formation of nonspherical clusters, and interparticle networks of spherical particles are the primary driver of the reduced viscosity η_r of monodisperse mixtures for particle volume fraction $\Phi > 0.05$. Thus, good agreement between the experimental data and unmodified viscosity models, which assume uniformly dispersed, rigid, spherical particles, only occurs for $\Phi < 0.05$. The presence of agglomerates violates the assumptions of "dilute" or "semidilute" models. Importantly, the experiments show that small particles elicited shear thinning/thixotropy due to particle deagglomeration, whereas large particles cause shear thickening/antithixotropy due to particle migration at high shear rates. 2) One must explicitly account for nonspherical clusters of spherical particles to improve agreement between monodisperse viscosity models and experimental data. This can be accomplished by modifying model parameters such as the fluidity limit Φ^* and the intrinsic viscosity $[\eta]$, which both change when accounting for anisotropy and by using a fractal approach. 3) Polydisperse mixtures are less viscous than monodisperse mixtures with the same particle volume fraction Φ. This is significant for high particle volume fraction, but we show that the effects are considerable at low particle volume fraction also, which is important in the context of mixtures of photopolymer and microparticles for VP. The fluidity limit Φ^* increases because the small particles fit in the voids between large particles until approximately $\Phi_s = 50\%$, thus reducing hydrodynamic interactions and collisions between particles. These findings are pertinent for determining optimal timescales of recovery after periods of high shear, such as during the VP recoating process. Furthermore, the results highlight that proper selection of particle dispersity is key to formulating mixture of photopolymer and microparticles for VP processes. 4) Although the viscosity experiments displayed similar trends to those predicted by existing viscosity models, we did not determine adequate agreement between experiments and models to substantiate their use in this context. For this reason, further improvement of these models, similar to the improvements made using a fractal approach for the monodisperse models, is a clear path for future research.

Acknowledgements

J.U., M.F., and B.R. acknowledge support of the National Science Foundation award CMMI-2130083.

Conflict of Interest

The authors declare no conflict of interest.

Data Availability Statement

The data that support the findings of this study are available from the corresponding author upon reasonable request.

Keywords

particle size distributions, photopolymers, rheology, vat polymerization, viscosity modeling

Received: October 5, 2023
Revised: December 13, 2023
Published online: March 22, 2024

[1] R. F. Gibson, *Principles of Composite Material Mechanics*, CRC Press, Boca Raton **2016**.
[2] Y. Ming, Z. Xin, J. Zhang, Y. Duan, B. Wang, *Compos. Commun.* **2020**, *21*, 100401.
[3] S. M. F. Kabir, K. Mathur, A.-F. M. Seyam, *Compos. Struct.* **2020**, *232*, 111476.
[4] N. P. Singh, V. K. Gupta, A. P. Singh, *Polymer* **2019**, *180*, 121724.
[5] B. Herren, P. Larson, M. C. Saha, Y. Liu, *Polymers* **2019**, *11*, 1212.
[6] M. D. Haslam, B. Raeymaekers, *Composites, Part B* **2014**, *60*, 91.
[7] W. Xu, S. Jambhulkar, D. Ravichandran, Y. Zhu, M. Kakarla, Q. Nian, B. Azeredo, X. Chen, K. Jin, B. Vernon, D. G. Lott, J. L. Cornella, O. Shefi, G. Miquelard-Garnier, Y. Yang, K. Song, *Small* **2021**, *17*, 2100817.
[8] B. Raeymaekers, *Design of Mechanical Elements: A Concise Introduction to Mechanical Design Considerations and Calculations*, John Wiley & Sons, Hoboken, NJ **2022**.
[9] A. J. Kennedy, A. D. McQueen, M. L. Ballentine, L. R. May, B. M. Fernando, A. Das, K. L. Klaus, C. B. Williams, M. J. Bortner, *Chem. Eng. J.* **2023**, *455*, 140866.
[10] T. Chartier, C. Chaput, F. Doreau, M. Loiseau, *J. Mater. Sci.* **2002**, *37*, 3141.
[11] R. Tu, H. A. Sodano, *Addit. Manuf.* **2021**, *46*, 102180.
[12] B. Panda, C. Unluer, M. J. Tan, *Cem. Concr. Compos.* **2018**, *94*, 307.
[13] I. Gibson, D. Rosen, B. Stucker, *Additive Manufacturing Technologies: 3D Printing, Rapid Prototyping, and Direct Digital Manufacturing* (Eds: I. Gibson, D. Rosen, B. Stucker), Springer, New York, NY **2015**, pp. 147–173.
[14] I. Gibson, D. Rosen, B. Stucker, *Additive Manufacturing Technologies: 3D Printing, Rapid Prototyping, and Direct Digital Manufacturing* (Eds: I. Gibson, D. Rosen, B. Stucker), Springer, New York, NY **2015**, pp. 63–106.
[15] K. Niendorf, B. Raeymaekers, *Adv. Eng. Mater.* **2021**, *23*, 2001002.
[16] D. Z. Gunes, R. Scirocco, J. Mewis, J. Vermant, *J. Non-Newton. Fluid Mech.* **2008**, *155*, 39.
[17] Y. Yang, X. Li, M. Chu, H. Sun, J. Jin, K. Yu, Q. Wang, Q. Zhou, Y. Chen, *Sci. Adv.* **2019**, *5*, eaau9490.
[18] R. M. Erb, J. Segmehl, M. Charilaou, J. F. Löffler, A. R. Studart, *Soft Matter* **2012**, *8*, 7604.
[19] J. Greenhall, B. Raeymaekers, *Adv. Mater. Technol.* **2017**, *2*, 1700122.
[20] M.-S. Scholz, B. W. Drinkwater, R. S. Trask, *Ultrasonics* **2014**, *54*, 1015.
[21] S. Noparast, F. Guevara Vasquez, B. Raeymaekers, *J. Appl. Phys.* **2022**, *131*, 134901.
[22] C. W. Macosko, *Rheology: Principles, Measurements, and Applications*, VCH, New York **1994**.
[23] J. Bicerano, J. F. Douglas, D. A. Brune, *J. Macromol. Sci. Part C: Polym. Rev.* **1999**, *39*, 561.

[24] J. Liang, M. Francoeur, C. B. Williams, B. Raeymaekers, *ACS Appl. Polym. Mater.* **2023**, *5*, 9017.
[25] B. P. Croom, A. Abbott, J. W. Kemp, L. Rueschhoff, L. Smieska, A. Woll, S. Stoupin, H. Koerner, *Addit. Manuf.* **2021**, *37*, 101701.
[26] A. Felt, B. Raeymaekers, *Addit. Manuf. Lett.* **2023**, *5*, 100120.
[27] D. A. Rau, M. Forgiarini, C. B. Williams, *Addit. Manuf.* **2021**, *42*, 101996.
[28] Z. Wu, W. Liu, H. Wu, R. Huang, R. He, Q. Jiang, Y. Chen, X. Ji, Z. Tian, S. Wu, *Mater. Chem. Phys.* **2018**, *207*, 1.
[29] T. Zhao, X. Li, R. Yu, Y. Zhang, X. Yang, X. Zhao, L. Wang, W. Huang, *Macromol. Chem. Phys.* **2018**, *219*, 1700530.
[30] K. Niendorf, B. Raeymaekers, *Composites, Part A* **2020**, *129*, 105713.
[31] K. Niendorf, B. Raeymaekers, *Composites, Part B* **2021**, *223*, 109096.
[32] S. Mazumdar, *Composites Manufacturing: Materials, Product, and Process Engineering*, CRC Press, Boca Raton **2001**.
[33] J. Greenhall, L. Homel, B. Raeymaekers, *J. Compos. Mater.* **2019**, *53*, 1329.
[34] Z. Chen, J. Li, C. Liu, Y. Liu, J. Zhu, C. Lao, *Ceram. Int.* **2019**, *45*, 11549.
[35] S. P. Gentry, J. W. Halloran, *J. Eur. Ceram. Soc.* **2013**, *33*, 1981.
[36] V. G. Kulichikhin, A. Y. Malkin, *Polymers* **2022**, *14*, 1262.
[37] A. Corker, H. C.-H. Ng, R. J. Poole, E. García-Tuñón, *Soft Matter* **2019**, *15*, 1444.
[38] R. G. Larson, Y. Wei, *J. Rheol.* **2019**, *63*, 477.
[39] F. Rubio-Hernández, J. Sánchez-Toro, N. Páez-Flor, *J. Rheol.* **2020**, *64*, 785.
[40] G. J. Kynch, *Br. J. Appl. Phys.* **1954**, *5*, S5.
[41] A. P. Shapiro, R. F. Probstein, *Phys. Rev. Lett.* **1992**, *68*, 1422.
[42] A. Einstein, *Ann. Phys.* **1911**, *339*, 591.
[43] H. C. Brinkman, *J. Chem. Phys.* **1952**, *20*, 571.
[44] G. K. Batchelor, J. T. Green, *J. Fluid Mech.* **1972**, *56*, 375.
[45] G. K. Batchelor, *J. Fluid Mech.* **1977**, *83*, 97.
[46] V. Vand, *J. Phys. Colloid Chem.* **1948**, *52*, 277.
[47] R. Roscoe, *Br. J. Appl. Phys.* **1952**, *3*, 267.
[48] I. M. Krieger, T. J. Dougherty, *Trans. Soc. Rheol.* **1959**, *3*, 137.
[49] C. I. Mendoza, I. Santamaría-Holek, *J. Chem. Phys.* **2009**, *130*, 044904.
[50] C. R. Wildemuth, M. C. Williams, *Rheol. Acta* **1984**, *23*, 627.
[51] C. G. de Kruif, E. M. F. van Iersel, A. Vrij, W. B. Russel, *J. Chem. Phys.* **1985**, *83*, 4717.
[52] J. C. van der Werff, C. G. de Kruif, *J. Rheol.* **1989**, *33*, 421.
[53] M. Mooney, *J. Colloid Sci.* **1951**, *6*, 162.
[54] J. S. Chong, E. B. Christiansen, A. D. Baer, *J. Appl. Polym. Sci.* **1971**, *15*, 2007.
[55] R. J. Farris, *Trans. Soc. Rheol.* **1968**, *12*, 281.
[56] R. Greenwood, P. F. Luckham, T. Gregory, *J. Colloid Interface Sci.* **1997**, *191*, 11.
[57] S. Pednekar, J. Chun, J. Morris, *J. Rheol.* **2018**, *62*, 513.
[58] S. A. Faroughi, C. Huber, *Phys. Rev. E* **2014**, *90*, 052303.
[59] P. Gondret, L. Petit, *J. Rheol.* **1997**, *41*, 1261.
[60] F. Qi, R. I. Tanner, *Korea-Aust. Rheol. J.* **2011**, *23*, 105.
[61] 3DRS Standard V2 Grey, 3D Resin Solution, https://3drs.com/products/3drs-standard-cool-grey-v2. (accessed: 29 August 2022).
[62] Soda Lime Solid Glass Microspheres 2.5g/Cc - Bulk with Coating Options - 3um to 75um, Cospheric, https://www.cospheric.com/P2000_solid_soda_lime_glass_spheres_beads.htm. (accessed: 29 August 2022).
[63] Novum Glass, https://www.novumglass.com/. (accessed: 29 August 2022).
[64] K. Remenárová, Study of Flow Behaviour of Conventional, Hybrid and UV Offset Inks, *Print. Future Days 2007*, *2007*, **2007**, p. 193.
[65] C.-J. Bae, J. W. Halloran, *J. Eur. Ceram. Soc.* **2019**, *39*, 4299.
[66] J. P. Reynolds, D. A. Rau, C. B. Williams, M. J. Bortner, *Addit. Manuf.* **2023**, *75*, 103753.
[67] Viscosity Correction: Weissenberg-Rabinowitsch-Mooney (WRM) - PDF Free Download, https://docplayer.net/203381741-Viscosity-correction-weissenberg-rabinowitsch-mooney-wrm.html. (accessed: 16 September 2021).
[68] M. M. Rueda, M.-C. Auscher, R. Fulchiron, T. Perie, G. Martin, P. Sonntag, P. Cassagnau, *Prog. Polym. Sci.* **2017**, *66*, 22.
[69] N. Willenbacher, K. Georgieva, Rheology of Disperse Systems, *Product Design and Engineering: Formulation of Gels and Pastes*, **2013**, pp. 7–49.
[70] J. Mewis, N. J. Wagner, *Adv. Colloid Interface Sci.* **2009**, *147*, 214.
[71] Y. Liu, Y. Lin, T. Jiao, G. Lu, J. Liu, *Polym. Chem.* **2019**, *10*, 6350.
[72] H. Chen, Y. Ding, Y. He, C. Tan, *Chem. Phys. Lett.* **2007**, *444*, 333.
[73] L. Guérin, C. Frances, A. Liné, C. Coufort-Saudejaud, *Colloids Surf. Physicochem. Eng. Asp.* **2019**, *560*, 213.
[74] Fractals & the Fractal Dimension, https://www.vanderbilt.edu/AnS/psychology/cogsci/chaos/workshop/Fractals.html. (accessed: 08 December 2022).
[75] C. Aubert, D. S. Cannell, *Phys. Rev. Lett.* **1986**, *56*, 738.
[76] R. A. Lionberger, *Phys. Rev. E* **2002**, *65*, 061408.
[77] R. D. Sudduth, *J. Appl. Polym. Sci.* **1993**, *48*, 37.